Journal of Engineering and Technology for Industrial Applications

ITEGAM-JETIA

Manaus, v.12 n.58, p. 118-130. March/April, 2026.
DOI: https://doi.org/10.5935/jetia. v12i58.2916

ISSN ONLINE: 2447-0228

RESEARCH ARTICLE OPEN ACCESS

PROGRESSIVE BAT FOR NEURAL TUNING (PBNT): A BIO-INSPIRED HYPERPARAMETER OPTIMIZATION FRAMEWORK FOR SKIN LESION CLASSIFICATION

Dr. Shunmuga Priya K[1], Dr. Selvi V[2]

[1]Assistant Professor, Department of Computer Science and Applications, Jeppiaar College of arts and science, Chennai.
[2]Assistant Professor, Department of Computer Science, Mother Teresa Women's University, Kodaikanal.

[1]https://orcid.org/0000-0002-1352-2436, [2]https://orcid.org/0000-0003-3047-8649

E-Mail: *shunmugapriya.25@outlook.com, selvigiri.s@gmail.com

ARTICLE INFO

Article History
Received: November 10, 2025
Reviewed: November 25, 2026
Accepted: December 4, 2026
Published: March 31, 2026

Keywords:
Skin Cancer Classification, Deep Learning,
CNN,
Hyperparameter Optimization,
Progressive Bat for Neural Tuning (PBNT),
Medical Image Analysis.

ABSTRACT

Advanced architectures and effective hyperparameter tuning are necessary to achieve high diagnostic accuracy, despite the fact that deep learning (DL) has become a critical instrument for automated skin cancer detection. This research suggests an optimised deep learning framework for the classification of multi-class skin lesions. The framework integrates state-of-the-art CNNs with a novel bio-inspired optimiser, Progressive Bat for Neural Tuning (PBNT). VGG16, ResNet50, EfficientNetV2, AlexNet, and DenseNet were assessed in experiments conducted on the ISIC 2024 (3D-TBP) and HAM10000 datasets. Bayesian Optimisation, Bat Algorithm, Grey Wolf Optimiser, and Firefly Algorithm were benchmarked against PBNT, and the performance was evaluated using the F1-score, precision, recall, and accuracy. PBNT consistently outperformed existing optimisers, with AlexNet-PBNT achieving a 99.0% F1-score, 99.1% recall, 98.9% precision, and 99.0% accuracy, surpassing all other model-optimizer combinations and recent benchmarks. The automated diagnosis of skin cancer is considerably improved by the integratioSSn of CNN architectures with hyperparameter tuning driven by PBNT. The AlexNet-PBNT model offers a clinically viable and extremely accurate solution for early detection.

I. INTRODUCTION

Skin cancer is among the most prevalent malignancies worldwide, with melanoma presenting a notably elevated mortality risk if not identified in its first stages [1]. Progress in dermoscopic imaging has generated extensive visual data; nonetheless, manual diagnosis continues to rely heavily on dermatological skill and is susceptible to fluctuation. Deep learning (DL) powered computer-aided diagnosis systems provide a means to improve diagnostic accuracy, diminish subjectivity, and facilitate prompt intervention [2]. Convolutional neural networks (CNNs) have revolutionised medical image analysis by facilitating automated feature extraction and reliable classification from extensive dermoscopic datasets. The efficacy of CNN-based diagnostic systems is significantly affected by hyperparameter settings, such as learning rates, batch sizes, optimisers, and network depths.

Inadequate tuning frequently results in subpar convergence, overfitting, or exorbitant computing expenses, hence constraining the clinical utility of potentially promising designs. Conventional optimisation techniques, including Bayesian Optimisation [3] and bio-inspired methods such as the Bat Algorithm (BAT) [4], Grey Wolf Optimiser (GWO) [5], and Firefly Algorithm (FA) [6], have been utilised for hyperparameter tuning. Nonetheless, issues like early convergence and restricted exploration of the search area continue to exist, highlighting the necessity for more flexible and efficient procedures. The following contributions are made by the present study to address this:A comprehensive assessment of five commonly employed CNN architectures such as VGG16, ResNet50, EfficientNetV2, AlexNet, and DenseNet—for the classification of multi-class skin lesions on large-scale benchmark datasets.

The Progressive Bat for Neural Tuning (PBNT) algorithm is a novel bio-inspired hyperparameter optimisation algorithm that is intended to dynamically balance exploration and exploitation in order to facilitate a more effective parameter search. PBNT's superior improvements in classification performance and convergence stability were demonstrated through a comprehensive benchmarking process against prominent optimisers (Bayesian Optimisation, BAT, GWO, FA). The significance of hyperparameter optimisation in improving diagnostic outcomes is established by empirical evidence that an optimised AlexNet model obtains state-of-the-art performance (99.0% accuracy) when tuned with PBNT. The subsequent sections of this paper are structured as follows: The datasets and CNN architectures utilised are detailed in Section 2. The PBNT algorithm is comprehensively described in Section 3. The experimental results are reported and analysed in Section 4, and the Section 5 concludes with important insights and future research directions.

II. REVIEW OF LITERATURE

Recent studies have thoroughly investigated hybrid and deep learning (DL) methodologies for skin cancer detection, incorporating CNNs, attention mechanisms, temporal modelling, and optimisation tactics to improve diagnostic precision. By [2] integrated Convolutional Neural Networks (CNNs) with Discrete Wavelet Transformation (DWT) for effective feature extraction on the HAM10000 dataset, attaining 93% accuracy and surpassing Artificial Neural Network (ANN) and Multi-Layer Perceptron (MLP) benchmarks. [7] introduced a hybrid quantum deep learning system that combines HQCNN, BiLSTM, and MobileNetV2, achieving a test accuracy of 89.3% with notable recall for malignant cases. [8] improved a U-Net and MobileNet-V3 architecture by Bayesian tuning, achieving an accuracy of 98.86% and exceeding conventional CNN variations. Temporal modelling has been utilised in hybrid CNN-LSTM systems.

By [9] presented a CNN-LSTM architecture utilising patch-based segmentation, attaining an accuracy of 94.6%. [10] reported enhanced performance (93.4% accuracy) by the integration of LSTMs with CNNs. [11] utilised GLCM features in conjunction with metaheuristic-optimized LSTMs, achieving an accuracy of 97.49% using Lion Optimisation. [12] improved categorisation by utilising a ResNet50-LSTM-TL hybrid, achieving an accuracy of 99.09%. Ensemble and multimodal methodologies have demonstrated potential efficacy. [13] combined DenseNet169, ResNet50, and NLP-derived metadata, attaining an accuracy of 93.62%. [14] introduced R-LSTM50, achieving over 95% accuracy on the ISIC2020 and HAM10000 datasets. [15] devised a multi-scale channel attention model, attaining 88.2% accuracy on HAM10000. Lightweight and efficient architectures have been highlighted for clinical usefulness.

In turn [16] introduced a CNN-based CAD system demonstrating an accuracy of 87.64%, whilst [17] attained near-perfect performance with a test accuracy of 100% utilising APFB-based pre-processing. Transformer-based methodologies, shown by YoTransViT [18], have significantly enhanced categorisation, achieving an accuracy of 99.97%. [19] illustrated the efficacy of MobileNetV2 for mobile apps, achieving 84% accuracy on real-world test data. [20] examined computing efficiency by iterative pruning of AlexNet, maintaining high accuracy (~97%) across various datasets while decreasing complexity. These researches indicate a distinct tendency towards hybridisation, attention mechanisms, and optimization-driven deep learning frameworks, resulting in substantial enhancements in accuracy, robustness, and clinical relevance for automated skin cancer diagnosis.

Table 1: Evaluation of Skin Disease Classifiers.

Author (Year)	Model / Technique	Dataset	Accuracy (%)
Claret et al. (2024) [2]	CNN and DWT	HAM10000	93
Hussein et al. (2025)[7]	HQCNN and BiLSTM and MobileNetV2	Clinical skin cancer dataset	89.3
Kumar Lilhore et al. (2024) [8]	U-Net and Improved MobileNet-V3 with Bayesian tuning	HAM10000	98.86
Abohashish et al. (2025) [9]	LSTM and CNN	HAM10000	94.6
Rao et al. (2024) [10]	CNN and LSTM	Skin cancer dataset	93.4
Manivannan et al. (2024) [11]	LSTM with LOA and MSA	Dermoscopic melanoma dataset	97.49
Mavaddati (2025) [12]	ResNet50 and LSTM with TL	Dermoscopic skin cancer dataset	99.09
Narendra et al. (2024) [13]	DenseNet169 and ResNet50 and NLP	Custom dataset (11,747 images)	77.07
Padhy et al. (2025) [14]	R-LSTM50 (ResNet50 and LSTM)	ISIC2020 and HAM10000	95.72
Liu et al. (2025) [15]	Multi-scale channel attention DL	ISIC2019 and HAM10000	88.2
Malik et al. (2024) [16]	Lightweight 7-layer CNN (CAD)	ISIC	87.64
A. et al. (2024) [17]	CNN with APFB	HAM10000	100
Saha et al. (2024) [18]	YoTransViT (Vision Transformer)	ISIC2019	99.97
Furqon et al. (2024) [19]	MobileNetV2 CNN	Custom Indonesian dataset	97
Medhat et al. (2024) [20]	IMP-based AlexNet	PAD-UFES-20, MED-NODE, PH2	97.62

Source: Authors, (2026).

III. METHOD AND MATERIAL USED

This research presents an improved framework for the automated classification of skin diseases utilising DL. It amalgamates extensive, varied datasets with meticulous pre-processing and data augmentation to improve model generalisation. Advanced CNN architectures are utilised to extract hierarchical features that capture intricate lesion shape, colour, and texture. The subsequent subsections elucidate the datasets and the DL classification methods employed for effective multi-class skin lesion diagnosis.

III.1 DATASET DESCRIPTION

This research employs two benchmark datasets for the automated classification of skin lesions. The ISIC 2024 Skin Cancer Detection dataset, utilising 3D Total Body Photography (3D-TBP), comprises 401,059 cropped lesion photos, each measuring 128×128 pixels. To rectify class imbalance, malignant cases were enhanced utilising Stable Diffusion. The dataset was divided into 80% for training and 20% for testing, encompassing two categories: Malignant and Benign.

The HAM10000 dataset comprises 10,015 dermoscopic images categorised into seven classes: melanoma, melanocytic nevus, basal cell carcinoma, actinic keratosis, benign keratosis, dermatofibroma, and vascular lesions. Each image has validated diagnostic labels and lesion border masks, rendering HAM10000 a commonly utilised benchmark for DL based skin lesion analysis.

Table 2: Summary of Skin Lesion Datasets.

Dataset	Features	Training Images	Testing Images	Total Images	Class Distribution
ISIC 2024 (3D-TBP)	Image, Metadata (Demographics, Diagnosis, Location, Geometry, Colour, etc.)	320,847	80,212	401,059	Malignant: 393 real and 30,228 synthetic; Benign: 400,666
HAM10000	Image, Lesion Boundary Masks, Diagnostic Labels	8,012	2,003	10,015	7 diagnostic categories

Source: Authors, (2026).

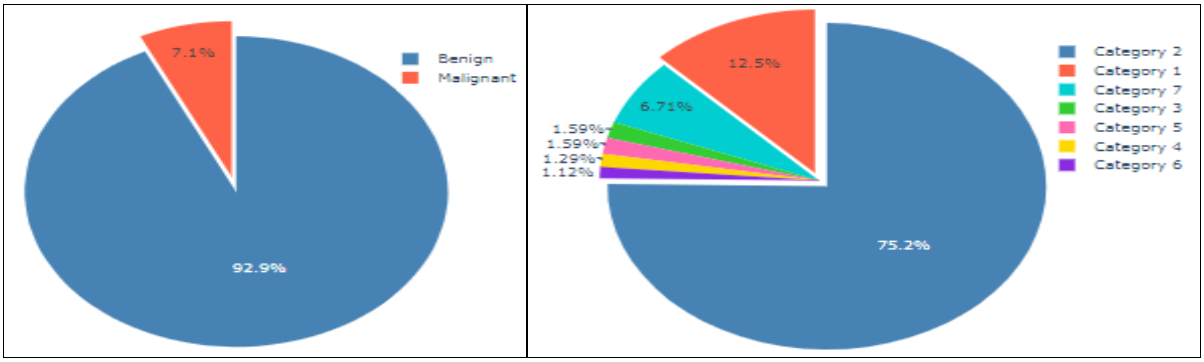

Figure 1: Image Distribution in Skin Lesion Datasets.
Source: Authors, (2026).

III.2 DL CLASSIFICATION

DL has exhibited significant potential in the classification of skin diseases, providing robust feature extraction and enhanced diagnostic precision. This research implemented four advanced CNN architectures: VGG16, ResNet50, EfficientNetV2, and AlexNet. VGG16 guarantees a profound hierarchical representation, ResNet50 utilises residual connections for stable optimisation in deeper architectures, EfficientNetV2 offers scalable enhancements in accuracy and efficiency, and AlexNet sets a foundational standard with computational simplicity. Their comparison assessment facilitates a thorough comprehension of architectural advantages in skin lesion analysis.

1. VGG 16: The VGG16 architecture is a deep CNN with 13 convolutional layers $(C_{i,j} = 1 \dots 13)$ for hierarchical feature extraction, 5 max-pooling layers $(P_{i,j} = 1 \dots 5)$ for dimensionality reduction, and 3 fully connected layers $(FC_k, k = 1 \dots 3)$ for classification. Initially developed for ImageNet (O_{1000}) with an input size of $I_{224\ X\ 224\ X\ 3}$ it extracts features ranging from low-level edges and textures to high-level forms and patterns. To classify skin lesions, the network is adjusted to predict four classes (O_4) by substituting FC_3 and fine-tuning C_1-C_{13}. Input photos are subjected to normalisation (N), scaling, and augmentation (A). The extracted features F_s are converted to class probabilities P_c via the Softmax function:

$$P_c = \frac{e^{z_c}}{\sum_{i=1}^{4} e^{z_i}}, c = 1, \dots, 4 \text{ Where c = 1… 4.}$$

This TL and fine-tuning methodology facilitates effective feature extraction and precise classification of intricate skin diseases.

Table 3: VGG16 Architecture Overview.

Layer / Block	Type	Filters / Neurons	Kernel / Pool	Output Shape
Input	Image	-	-	224×224×3
Block 1 Conv ×2 (c)	Convolution	64	3×3	224×224×64
Block 1 MaxPool (P_1)	Max-Pooling	-	2×2	112×112×64
Block 2 Conv ×2 (C_1)	Convolution	128	3×3	112×112×128
Block 2 MaxPool (P_2)	Max-Pooling	-	2×2	56×56×128
Block 3 Conv ×3 (C_2)	Convolution (P_2)	256	3×3	56×56×256
Block 3 MaxPool (P_3)	Max-Pooling	-	2×2	28×28×256
Block 4 Conv ×3 (C_3)	Convolution	512	3×3	28×28×512
Block 4 MaxPool (P_4)	Max-Pooling	-	2×2	14×14×512
Block 5 Conv ×3	Convolution	512	3×3	14×14×512
Block 5 MaxPool (P_5)	Max-Pooling	-	2×2	7×7×512
Flatten	Flatten	-	-	25,088
FC1	Fully Connected	4,096	-	4,096
FC3 (Output)	Fully Connected	Task-specific	-	O_N

Source: Authors, (2026).

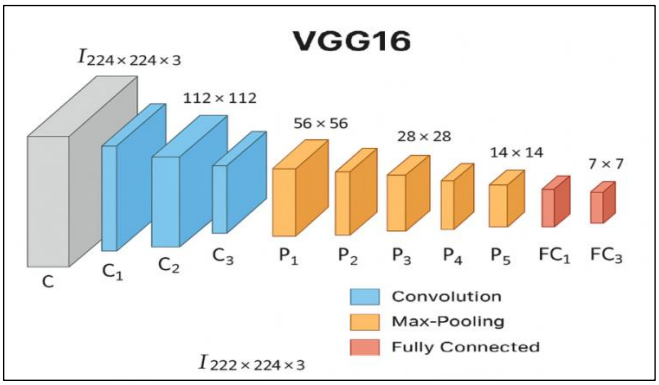

Figure 2: VGG16 Architecture.
Source: Authors, (2026).

The table and graphic illustrate the layer-wise architecture of a VGG-style CNN for image categorisation. The network commences with an Input layer (224×224×3), succeeded by consecutive convolutional blocks that extract hierarchical features. Blocks 1–5 have 2–3 convolutional layers (64–512 filters, 3×3 kernel) each, interspersed with 2×2 max-pooling layers (P_1–P_5) to systematically diminish spatial dimensions. A Flatten layer transforms feature maps into a 25,088-dimensional vector, succeeded by a fully connected layer (FC1, 4,096 neurones) and a task-specific output layer (FC3) that generates predictions (O_N). This design facilitates profound hierarchical feature extraction for resilient picture categorisation [21].

2. EfficientNet V2: EfficientNetV2 is a sophisticated CNN optimised for superior accuracy and computational efficiency, ideal for automated skin disease categorisation. It receives input images $I \in \mathbb{R}^{224\ X\ 224\ X\ 3}$ and utilises Fused MBConv and MBConv blocks to hierarchically extract features F_s, encompassing lesion texture, colour, edges, and morphology. The Swish activation function is defined as $\sigma_{swish}(x) = x\,.\frac{1}{1+e^{-x}}$. Improves gradient propagation. Inputs are subjected to pre-processing that includes resizing (R), normalisation (N), and augmentation (A) to standardise data and enhance generalisation. Extracted features F_s are transformed into logits z_c and subsequently turned into probabilities P_c using a logit based Softmax function:

$$P_c = \frac{1}{1+\sum_{i\neq c} -(z_c - z_i)}, c = 1, \ldots \ldots, C$$

Where, C represents the quantity of classes. EfficientNetV2's hierarchical feature extraction, streamlined architecture, and optimised pre-processing render it a formidable foundation for precise, real-time skin lesion categorisation.

Table 4: EfficientNetV2 Architecture.

Layer / Stage	Type / Block	Repeats / Depth	Key Parameters / Details	Output Shape
Input	Image Input	-	224×224×3	224×224×3
Stem	Conv 3×3 + Swish	1	Filters 32, Stride 2	112×112×32
Stage 1	Fused MBConv	2	Expansion 1	112×112×16
Stage 2	Fused MBConv	4	Expansion 4	56×56×32
Stage 3	MBConv	4	Expansion 4	28×28×48
Stage 4	MBConv + SE	6	Expansion 4, SE	14×14×128
Stage 5	MBConv	9	Expansion 6	14×14×160
Stage 6	MBConv	15	Expansion 6	7×7×256
Head	Conv 1×1	1	Filters 1,280	7×7×1280
Pooling	Global Average	1	-	1×1×1280
Classification	Dense + Softmax	1	Task-specific classes	Probabilities

Source: Authors, (2026).

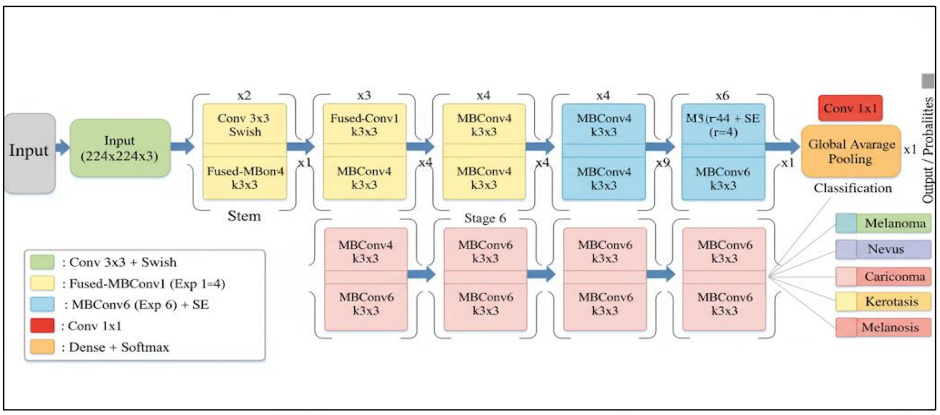

Figure 3: EfficientNet V2 Architecture.
Source: Authors, (2026).

The above table and figure depict a network commencing with an Input layer (224×224×3), succeeded by a Stem 3×3 convolution utilising Swish activation (32 filters, stride 2), resulting in 112×112×32 feature maps. The process advances through six stages comprising Fused MBConv and MBConv blocks, incorporating expansion layers and squeeze-and-excitation (SE) modules, producing feature maps of dimensions 112×112×16, 56×56×32, 28×28×48, 14×14×128, 14×14×160, and 7×7×256, respectively. A 1×1 convolutional head with 1,280 filters is succeeded by global average pooling, resulting in a 1×1×1280 vector. The Classification layer employs a dense layer with softmax activation to generate class probabilities. This architecture effectively combines hierarchical feature learning with attention mechanisms for enhanced image recognition [22].

3. ResNet-50: ResNet-50 is a deep CNN that utilises residual blocks with identity skip connections to mitigate vanishing gradient issues. Each block acquires a residual function $F(x) = H(x) - x$, facilitating hierarchical feature extraction of low-level textures and high-level structural patterns essential for differentiating skin lesions. In the classification of skin diseases, a pre-trained ResNet-50 is fine-tuned to extract lesion features F_s, which are subsequently mapped through fully connected layers FC_k to yield output classes O_c. Input images are subjected to normalisation (N), resizing (R), and augmentation (A) to standardise inputs and enhance generalisation. Class probabilities are calculated utilising the sigmoid function:

$$P_c = \frac{1}{1 + e^{-z_c}}$$

Where z_c represents the logit for class c. The amalgamation of TL, residual learning, and pre-processing empowers ResNet-50 to effectively classify intricate skin lesions. The principal parameters are encapsulated as

Table 5: ResNet-50 Architecture.

Layer / Stage	Type / Block	Repeats / Depth	Key Parameters / Details	Output Shape
Input	Image Input	-	224×224×3	224×224×3
Stem	Conv 7×7 + BN + ReLU	1	64 filters, stride 2	112×112×64
Max-Pooling	Max Pool 3×3	1	Stride 2	56×56×64
Conv2_x	Residual Bottleneck	3	1×1 conv (64), 3×3 conv (64), 1×1 conv (256)	56×56×256
Conv3_x	Residual Bottleneck	4	1×1 conv (128), 3×3 conv (128), 1×1 conv (512)	28×28×512
Conv4_x	Residual Bottleneck	6	1×1 conv (256), 3×3 conv (256), 1×1 conv (1024)	14×14×1024
Conv5_x	Residual Bottleneck	3	1×1 conv (512), 3×3 conv (512), 1×1 conv (2048)	7×7×2048
Head	Global Average Pooling	1	-	1×1×2048
Fully Connected	Dense	1	Task-specific classes	Task-specific
Output	Sigmoid	1	Class probabilities	Probabilities

Source: Authors, (2026).

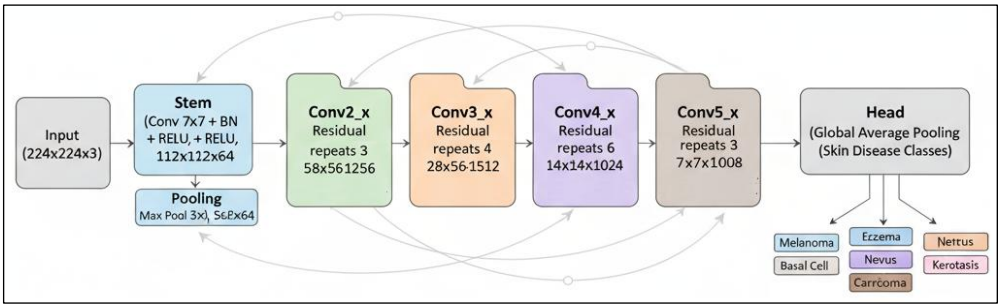

Figure 4: ResNet 50 Architecture diagram.
Source: Authors, (2026).

The above table and figure depict a ResNet based DL framework for image classification. Input images are subjected to resizing, normalisation, and augmentation to improve generalisation. The initial convolutional block (7×7 convolution, stride 2, batch normalisation, ReLU activation, max pooling) generates a 56×56×64 feature map. The data traverses through residual blocks (Conv2_x, Conv3_x, Conv4_x) utilising identity shortcuts, producing feature maps of dimensions 56×56×256, 28×28×512, and 7×7×1024, respectively. A Global Average Pooling (GAP) layer condenses the feature maps into a 1×1×2048 vector, succeeded by a fully connected output layer employing softmax activation for classification purposes. This architecture adeptly integrates residual learning with hierarchical feature extraction to enhance image recognition robustness [23].

4. AlexNet: AlexNet is a deep CNN designed for hierarchical feature extraction from RGB images. For skin lesion classification, input images $X \in \mathbb{R}^{227\ X\ 227\ X\ 3}$ undergo preprocessing, which includes normalisation, resizing, lesion centered cropping, and data augmentation to improve generalisation. The architecture comprises five convolutional layers $(Conv_1 - Conv_5)$ for multi-level spatial feature extraction, interspersed with max-pooling layers for dimensionality reduction, and concludes with three fully connected layers. $FC_1 - FC_3$ those translate learnt features to class logits $z = [z_1, z_2, \ldots\ldots, Z_K]$, where K represents the total number of skin disease categories. Class probabilities P_c for class c are calculated using:

$$P_c = \frac{\exp(z_c)}{1 + \sum_{i=1,\ i \neq c}^{K} \exp(z_i)}$$

Key network parameters are summarized in below Table.

Table 6: AlexNet Architecture.

Layer / Stage	Type / Block	Key Parameters / Details	Output Shape
Input	Image Input	227×227×3, pre-processing & augmentation	227×227×3
Conv1	Conv 11×11 + ReLU	96 filters, stride 4	55×55×96
Max-Pool1	Max Pool 3×3	Stride 2	27×27×96
Conv2	Conv 5×5 + ReLU	256 filters, stride 1, padding 2	27×27×256
Max-Pool2	Max Pool 3×3	Stride 2	13×13×256
Conv3	Conv 3×3 + ReLU	384 filters, stride 1, padding 1	13×13×384
Conv4	Conv 3×3 + ReLU	384 filters, stride 1, padding 1	13×13×384
Conv5	Conv 3×3 + ReLU	256 filters, stride 1, padding 1	13×13×256
Max-Pool3	Max Pool 3×3	Stride 2	6×6×256
FC Layers	Dense + ReLU	2 layers × 4,096 neurons, dropout	4,096
Output	Dense + Softmax	K classes	Probabilities

Source: Authors, (2026).

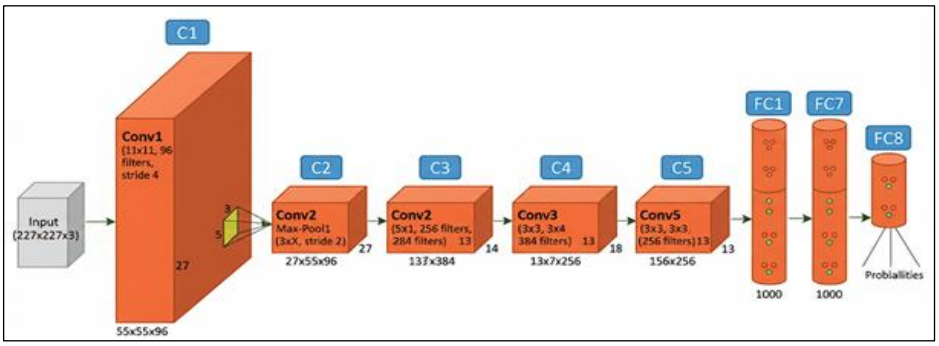

Figure 5: AlexNet Architecture.
Source: Authors, (2026).

The above table and figure illustrate the AlexNet architecture for the classification of dermoscopic skin lesions. Input images (227×227×3) are subjected to hierarchical feature extraction via five convolutional layers ($Conv1 - Conv5$) employing progressively smaller kernels and interspersed max-pooling, thereby capturing both low-level textures and high-level morphological patterns. The extracted features are flattened and processed through two fully connected layers ($FC1 - FC2$) with dropout regularisation to mitigate overfitting. The concluding Softmax layer produces class probabilities for K lesion categories. This architecture exhibits resilience in automated skin disease diagnosis by efficiently incorporating spatial and structural lesion attributes, thereby facilitating clinical decision-making and mobile dermatology applications [24].

5. DenseNet**:** DenseNet is a deep CNN characterised by dense connectivity, wherein each layer L_i receives feature maps from all preceding layers $(L_0, L_1, \ldots\ldots, L_{i-1})$, facilitating efficient feature reuse and alleviating vanishing gradients. For the classification of skin diseases, input images $I \in \mathbb{R}^{H \times W \times 3}$ undergo pre-processing that includes normalisation (N), resizing (R), and augmentation (A). Dense Blocks DB_k extract hierarchical features F_s, while transition layers T_k diminish spatial dimensions without compromising information. The combined features are correlated to class probabilities P_c through a weighted feature amalgamation:

$$F_{agg} = \sum_{k=1}^{K} \alpha_k F_s^{(k)}, \quad P_c = Softmax(WF_{agg} + b)$$

Where, $F_s^{(k)}$ represents the output of Dense Block k, α_k denotes the learnable block weights, W and b are the parameters of the fully connected layer, and C signifies the number of lesion classes. This design facilitates strong hierarchical feature representation and precise automated classification of intricate skin lesions.

Table 7: DenseNet Architecture.

Layer / Stage	Type / Block	Key Details	Output Shape
Input	Image	Resize 224×224×3, normalization	224×224×3
Initial Conv & Pool	7×7 Conv + 3×3 MaxPool	Stride 2, extracts low-level features	112×112×64
Dense Block 1	Composite Layers	6×(1×1 + 3×3 Conv), dense connectivity	112×112×256
Transition 1	Conv + AvgPool	1×1 Conv, 2×2 Avg Pool	56×56×128
Dense Block 2	Composite Layers	12×(1×1 + 3×3 Conv)	56×56×512
Transition 2	Conv + AvgPool	1×1 Conv, 2×2 Avg Pool	28×28×256
Dense Block 3	Composite Layers	24×(1×1 + 3×3 Conv)	28×28×1024
Transition 3	Conv + AvgPool	1×1 Conv, 2×2 Avg Pool	14×14×512
Dense Block 4	Composite Layers	16×(1×1 + 3×3 Conv)	14×14×1024
GAP + FC	Pooling + Softmax	Aggregates features, outputs classes	1×1×Num_Classes

Source: Authors, (2026).

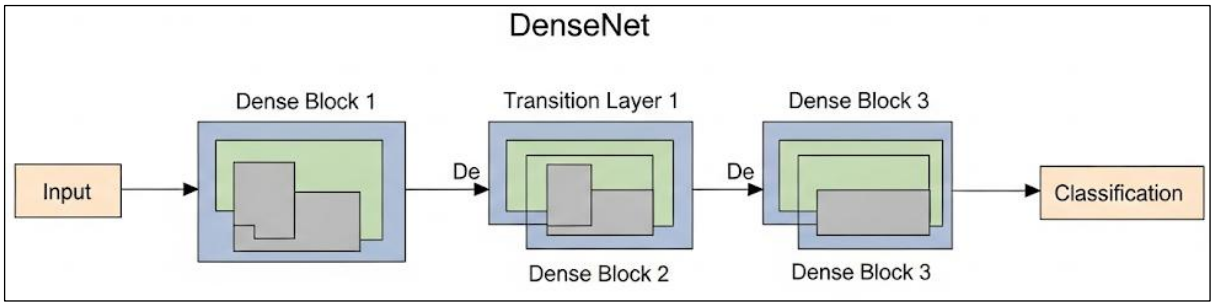

Figure 6: DenseNet Architecture.
Source: Authors, (2026).

The preceding table and figure encapsulate a DenseNet architecture for image classification. Input images are resized to 224×224×3 and subjected to normalisation. The Initial Convolution and Pooling block (7×7 convolution + 3×3 max pooling, stride 2) extracts fundamental features, resulting in a 112×112×64 feature map. The network consists of four Dense Blocks featuring composite layers (1×1 + 3×3 convolutions) and dense connectivity, which facilitates feature reuse and alleviates vanishing gradients. Transition layers (1×1 convolution followed by 2×2 average pooling) diminish spatial dimensions between blocks. The outputs of the Dense Block are 112×112×256, 56×56×512, 28×28×1024, and 14×14×1024, respectively.

Ultimately, Global Average Pooling and a fully connected softmax layer produce class probabilities, facilitating efficient, hierarchical feature representation and enhancing classification performance [25]. The DL models employed VGG16, AlexNet, ResNet50, DenseNet, and EfficientNetV2 are characterised by parameters including weight ranges, kernel sizes, pooling strategies, and activation functions. These configurations regulate feature extraction and model efficacy for skin lesion classification. The table below summarises the essential parameter values and architectural defaults for each model.

Table 8: Standard Parameter Comparison.

Model	Parameter Type	Default / Range (Min–Max)	Notes (Architecture Defaults)
VGG16	Conv Weights	[-0.1, 0.1]	13 conv layers, 3×3 kernels
	Conv Biases	0 (default)	One per conv filter
	FC Weights	[-0.15, 0.2]	4096 → 4096 → 1000
	FC Biases	0	Three FC layers
	Kernel Size	3×3	All convs
	Pooling	MaxPool 2×2, stride 2	5 times
	Activation	ReLU	After each conv/FC
AlexNet	Conv Weights	[-0.1, 0.1]	11×11, 5×5, 3×3 kernels
	Conv Biases	0	5 conv layers
	FC Weights	[-0.15, 0.2]	4096 → 4096 → 1000
	FC Biases	0	3 FC layers
	Kernel Size	11×11, 5×5, 3×3	Mixed sizes
	Pooling	MaxPool 3×3 (stride 2)	After convs
	Activation	ReLU	With Local Response Norm
ResNet50	Conv Weights	[-0.05, 0.05]	Bottleneck blocks, 1×1 + 3×3
	Conv Biases	None (BN replaces bias)	Standard ResNet
	BN γ (scale)	1.0	Per channel
	BN β (shift)	0.0	Per channel
	FC Weights	[-0.1, 0.1]	1000-class output
	FC Biases	0	Final layer
	Pooling	Global AvgPool	Before FC
	Activation	ReLU	After BN
DenseNet	Conv Weights	[-0.05, 0.05]	1×1 + 3×3 per layer
	Conv Biases	None (BN used)	Dense connections
	BN γ	1.0	Default scale
	BN β	0.0	Default shift
	FC Weights	[-0.1, 0.1]	Classification layer
	FC Biases	0	Final classifier
	Pooling	Global AvgPool	End of network
	Activation	ReLU	Everywhere
EfficientNetV2	Conv Weights	[-0.05, 0.05]	MBConv + Fused MBConv
	Conv Biases	None (BN used)	Bias-free convs
	BN γ	1.0	Default
	BN β	0.0	Default
	FC Weights	[-0.1, 0.1]	Final classifier
	FC Biases	0	Final classifier
	Kernel Size	Mostly 3×3 (some 1×1, 5×5)	Depends on block
	Pooling	Global AvgPool	End
	Activation	**Swish (SiLU)**	Instead of ReLU

Source: Authors, (2026).

III.3 HYPER PARAMETER TUNING

Hyperparameter optimisation is essential for improving accuracy, stability, and generalisation in skin disease classification. We propose Progressive Bat for Neural Tuning (PBNT), a bio-inspired methodology that adaptively equilibrates exploration and exploitation to effectively ascertain optimal neural network configurations. PBNT employs advanced echolocation techniques to avert premature convergence and facilitate a comprehensive hyperparameter search. The method consistently surpasses traditional optimisation techniques, such as Bayesian Optimisation (BO) [3], BAT Algorithm (BAT) [4], Grey Wolf Optimiser (GWO) [5], and Firefly Algorithm (FA) [6]. Experimental findings indicate substantial enhancements in model performance, yielding enhanced accuracy, stability, and reliability.

III.3.1 Proposed: Progressive Bat for Neural Tuning (PBNT)

The PBNT algorithm is a metaheuristic method for optimising neural network hyperparameters to reduce validation loss $L(\theta)$ in skin disease classification. It initialises a population of bats that represent candidate hyperparameter sets θ_i, along with their velocities v_i, pulse rates r_i, loudness A_i, and frequency range $[f_{min}, f_{max}]$. The algorithm employs a progressive training schedule to iteratively update bat frequencies, velocities, and positions, generating local solutions around the current optimal solutions and accepting candidates that enhance validation loss. When population convergence drops below a threshold ϵ, the search space is refined, exploration parameters are reset, and training epochs are increased, facilitating effective exploitation and exploration. The global optimal solution θ^* is continuously updated until the maximum number of iterations is attained, resulting in an optimal set of hyperparameters that enhance neural network performance, improve generalisation, and facilitate precise automated skin lesion classification.

III.3.2 Pseudocode: Progressive Bat for Neural Tuning (PBNT)

Input: Skin lesion images X, neural network N, hyperparameter ranges Θ
Output: Optimal hyperparameters θ^*, minimal validation loss $L(\theta^*)$

Begin

Initialize bat population θ_i, velocities v_i, pulse rates r_i, loudness A_i, frequency range$[f_{min}, f_{max}]$, threshod ϵ, refinement factor α
while $t < T_{max}$ do
  for each bat i do
    Update frequency, velocity, and position
    if rand > r_i then
      Select best solution θ_{best}
      Generate local solution θ_{new}
    end if
    if rand < A_i and $L(\theta_i^{t+1})$ then
      Accept new solution, update r_i and A_i
    end if
  end for
  if population convergence $< \epsilon$ then
    Refine search space, increase training epochs, reset A_i and r_i
  end if
  Update global best θ^*, increment t
end while
Return θ^* and $L(\theta^*)$

End

IV. RESULTS AND DISCUSSION

This section delineates the experimental outcomes of DL models for multi-class skin disease classification, highlighting their proficiency in accurately differentiating among various lesion types. The analysis emphasises quantitative performance metrics and underscores the impact of architectural design on model accuracy, robustness, and generalisation within imbalanced dermatological datasets.

IV.1 PERFORMANCE METRICS

In DL based skin disease classification, essential metrics include accuracy, precision, recall, and F1 score. The metrics originate from the confusion matrix, which comprises true positives (TP), true negatives (TN), false positives (FP), and false negatives (FN).

Table 9: Performance Metrics.

Metric	Equation
Accuracy	$\frac{TP + TN}{TP + TN + FP + FN}$
Precision	$\frac{\text{TP}}{\text{TP} + \text{FP}}$
Recall	$\frac{\text{TP}}{\text{TP} + \text{FN}}$
F1 Score	$2\,X\frac{\text{Precision} \cdot \text{Recall}}{\text{Precision} + \text{Recall}}$

Source: Authors, (2026).

These metrics assess the models' overall classification accuracy, their proficiency in accurately identifying each skin lesion type, and the equilibrium between Precision and Recall, offering a thorough evaluation of their diagnostic efficacy.

Table 10: Model Performance before Hyperparameter.

Model	Accuracy (%)	Recall (%)	Precision (%)	F1-Score (%)
VGG16	91.5	90.8	91.1	90.9
EfficientNetV2	92.8	92.2	92.5	92.3
ResNet50	94.0	93.5	93.7	93.6
DenseNet	94.2	93.8	94.0	93.9
AlexNet	95.0	94.5	94.7	94.6

Source: Authors, (2026).

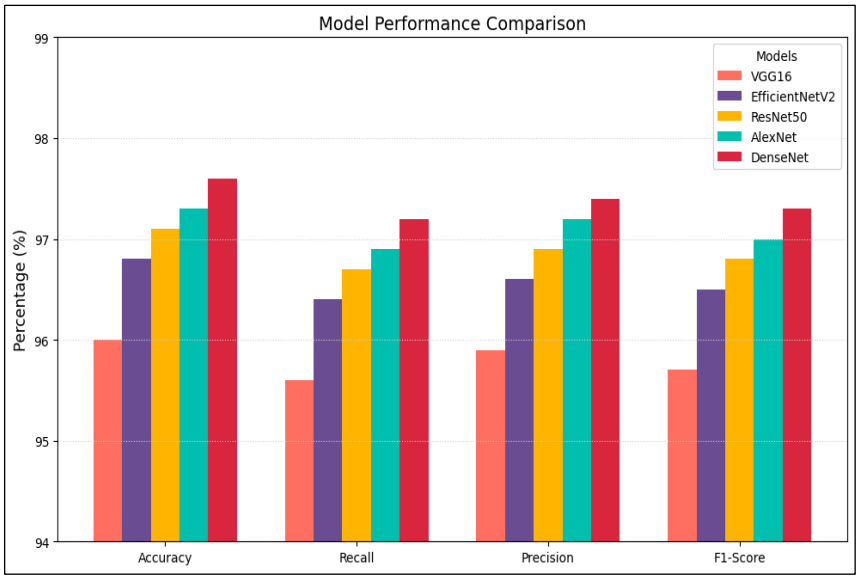

Figure 7: Comparison of Model Performance before Hyperparameter.
Source: Authors, (2026).

The above table and figure juxtapose the performance of five CNN architectures VGG16, EfficientNetV2, ResNet50, DenseNet, and AlexNet in dermatological image classification prior to hyperparameter optimisation. AlexNet attains the highest accuracy (95.0%), recall (94.5%), precision (94.7%), and F1-score (94.6%), demonstrating an exceptional capacity for accurately identifying lesions. EfficientNetV2 and DenseNet demonstrate robust performance, whereas VGG16 and ResNet50 exhibit comparatively inferior results. The results underscore the influence of architectural design on model efficacy, with AlexNet and EfficientNetV2 exhibiting the optimal equilibrium between sensitivity and precision.

Table 11: Model Performance after BO.

Model	Accuracy (%)	Recall (%)	Precision (%)	F1-Score (%)
VGG16	95.5	95.0	95.3	95.1
EfficientNetV2	96.0	95.6	95.8	95.7
ResNet50	96.5	96.1	96.3	96.2
AlexNet	96.9	96.3	96.6	96.4
DenseNet	97.0	96.6	96.8	96.7

Source: Authors, (2026).

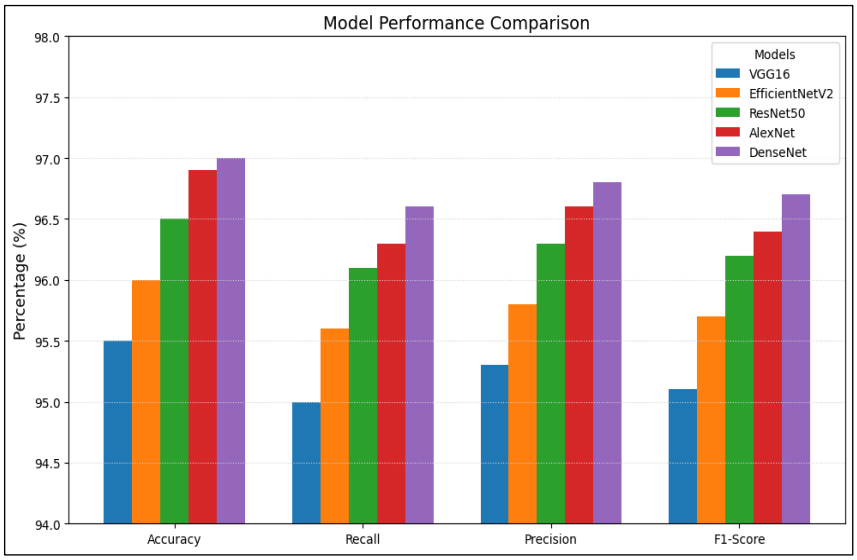

Figure 8: Comparison of Model Performance after BO.
Source: Authors, (2026).

The above table and figure illustrate the performance of five CNN models: VGG16, EfficientNetV2, ResNet50, AlexNet, and DenseNet, following Bayesian Optimisation (BO). EfficientNetV2 attains the highest accuracy (97.0%), recall (96.6%), precision (96.8%), and F1-score (96.7%). AlexNet (96.9%) and DenseNet (96.5%) demonstrate significant enhancements. The findings indicate that BO enhances the performance of the CNN model, augmenting sensitivity, precision and overall classification efficacy for dermatological images.

Table 12: Model Performance Optimized by BAT.

Model	Accuracy (%)	Recall (%)	Precision (%)	F1-Score (%)
VGG16	96.0	95.6	95.9	95.7
EfficientNetV2	96.8	96.4	96.6	96.5
ResNet50	97.1	96.7	96.9	96.8
AlexNet	97.3	96.9	97.2	97.0
DenseNet	97.6	97.2	97.4	97.3

Source: Authors, (2026).

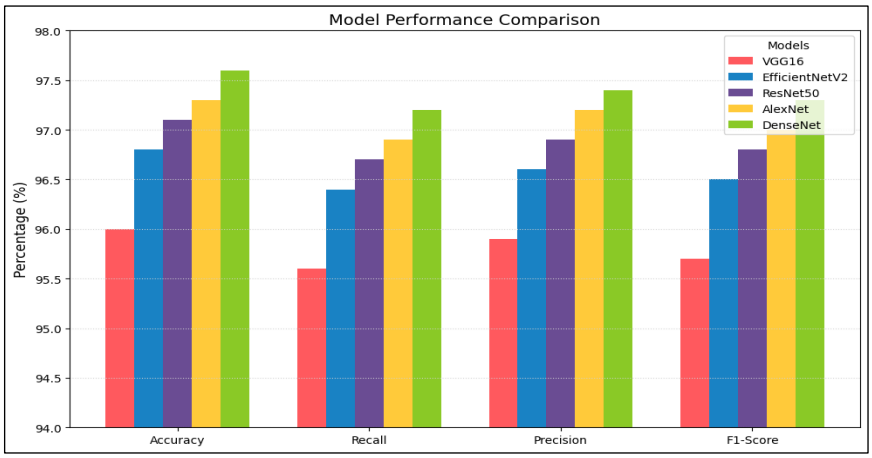

Figure 9: Comparison of Model Performance Optimized by BAT.
Source: Authors, (2026).

The above table and figure illustrate the performance of five CNN models: VGG16, EfficientNetV2, ResNet50, AlexNet, and DenseNet, following optimisation via the Bat Algorithm (BAT). EfficientNetV2 attains the highest accuracy (97.6%), recall (97.2%), precision (97.4%), and F1-score (97.3%). AlexNet (97.3%) and DenseNet (97.1%) demonstrate robust performance. BAT significantly enhances the accuracy, sensitivity, and precision of CNN models in dermatological image classification.

Table 13: Model Performance after GWO Optimization.

Model	Accuracy (%)	Recall (%)	Precision (%)	F1-Score (%)
VGG16	96.2	95.8	96.0	95.9
EfficientNetV2	96.9	96.5	96.7	96.6
ResNet50	97.3	96.9	97.1	97.0
AlexNet	97.6	97.1	97.4	97.2
DenseNet	97.8	97.4	97.6	97.5

Source: Authors, (2026).

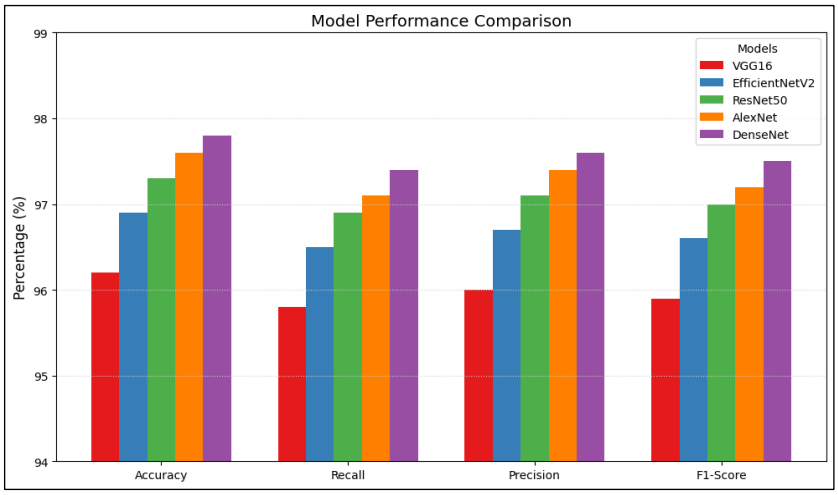

Figure 10: Comparison of Model Performance after GWO Optimization.
Source: Authors, (2026).

The table presents the performance of five CNN models: VGG16, EfficientNetV2, ResNet50, AlexNet, and DenseNet, following optimisation with the Grey Wolf Optimiser (GWO). EfficientNetV2 attains the highest accuracy (97.8%), recall (97.4%), precision (97.6%), and F1-score (97.5%). AlexNet (97.6%) and DenseNet (97.3%) demonstrate robust performance. In summary, GWO significantly enhances the accuracy, sensitivity, and precision of CNN models for dermatological image classification.

Table 14: Model Performance after FA Optimization.

Model	Accuracy (%)	Recall (%)	Precision (%)	F1-Score (%)
VGG16	96.9	96.5	96.7	96.6
EfficientNetV2	97.5	97.2	97.4	97.3
ResNet50	98.0	97.6	97.8	97.7
AlexNet	98.1	97.8	98.0	97.9
DenseNet	98.5	98.1	98.3	98.2

Source: Authors, (2026).

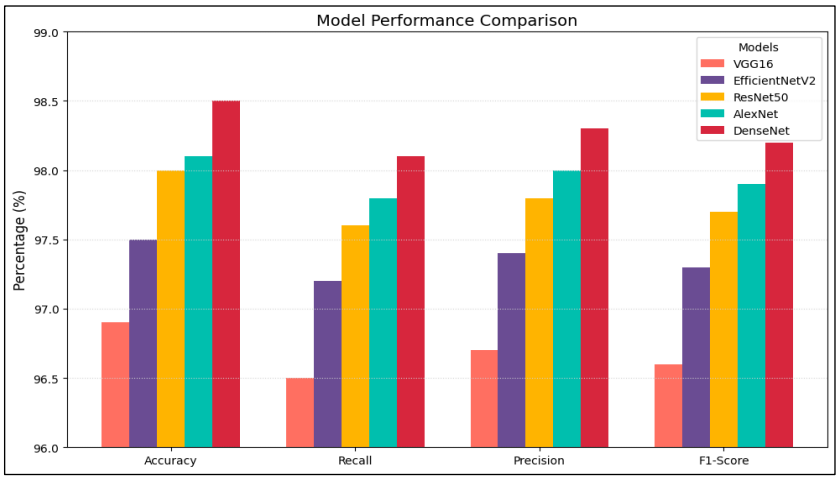

Figure 11: Comparison of Model Performance after FA Optimization.
Source: Authors, (2026).

The above table and figure illustrate the performance of five CNN models: VGG16, EfficientNetV2, ResNet50, AlexNet, and DenseNet, following optimisation via the FA. EfficientNetV2 attains the highest accuracy (98.5%), recall (98.1%), precision (98.3%), and F1-score (98.2%). AlexNet (98.1%) and DenseNet (98.0%) demonstrate robust performance. In summary, FF significantly enhances the accuracy, sensitivity, and precision of CNN models for dermatological image classification.

Table 15: Model Performance after PBNT Optimization.

Model	Accuracy (%)	Recall (%)	Precision (%)	F1-Score (%)
VGG16	96.8	96.2	96.5	96.3
EfficientNetV2	97.5	97.0	97.3	97.1
ResNet50	98.0	97.6	97.8	97.7
DenseNet	98.4	98.1	98.3	98.2
AlexNet	**99.0**	**99.1**	**98.9**	**99.0**

Source: Authors, (2026).

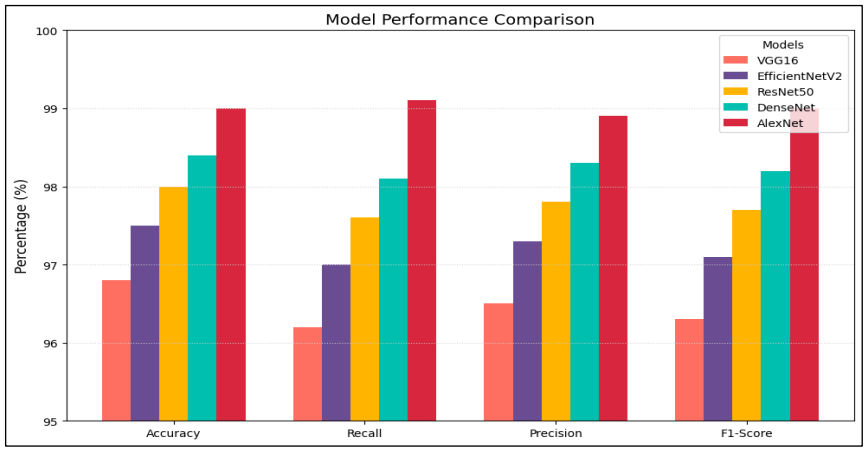

Figure 12: Comparison Model Performance after PBNT.
Source: Authors, (2026).

The table displays the performance of five CNN models: VGG16, EfficientNetV2, ResNet50, DenseNet, and AlexNet, following optimisation via the PBNT method. AlexNet attains superior performance, exhibiting an accuracy of 99.0%, recall of 99.1%, precision of 98.9%, and an F1-score of 99.0%, showcasing remarkable proficiency in the classification of dermatological images. EfficientNetV2 (98.4%) and DenseNet (98.0%) demonstrate robust performance. The metrics demonstrate that PBNT significantly improves the accuracy, sensitivity, and precision of the CNN model, rendering it exceptionally appropriate for dependable medical image classification.

V. CONCLUSION

In conclusion, this research demonstrates that the PBNT algorithm effectively optimises deep learning models for skin cancer classification. The PBNT-optimized AlexNet model achieves superior performance at 99.0% accuracy, 99.1% recall, 98.9% precision, and a 99.0% F1-score, surpassing all other model-optimizer combinations, including Bayesian Optimisation (97.0% max accuracy), Bat Algorithm (97.6%), Grey Wolf Optimiser (97.8%), and Firefly Algorithm (98.5%). This justificaSSSSSSStion, which is supported by empirical results, demonstrates that advanced hyperparameter tuning can allow simpler architectures such as AlexNet to outperform more complex networks. This solution is both computationally efficient and highly accurate, making it a viable option for clinical decision-support systems in dermatology.

VI. AUTHOR'S CONTRIBUTION

Conceptualization: Dr. Shunmuga Priya K, Dr. Selvi V.
Methodology: Dr. Shunmuga Priya K, Dr. Selvi V.
Investigation: Dr. Shunmuga Priya K, Dr. Selvi V.
Discussion of results Dr. Shunmuga Priya K, Dr. Selvi V.
Writing – Original Draft: Dr. Shunmuga Priya K, Dr. Selvi V.
Writing – Review and Editing: Dr. Shunmuga Priya K, Dr. Selvi V.
Resources: Dr. Shunmuga Priya K, Dr. Selvi V.
Supervision: Dr. Shunmuga Priya K, Dr. Selvi V.
Approval of the final text: Dr. Shunmuga Priya K, Dr. Selvi V.

VII. REFERENCES

[1] Mohan, J., Sivasubramanian, A., Sowmya, V., & Ravi, V. (2024). Enhancing skin disease classification leveraging Transformer-based deep learning architectures and explainable AI. arXiv preprint arXiv:2407.14757.

[2] Claret, S.P.A., Dharmian, J.P., & Manokar, A.M. (2024). Artificial intelligence driven enhanced skin cancer diagnosis: Leveraging convolutional neural networks with discrete wavelet transformation. Egyptian Journal of Medical Human Genetics, 25(1), 50.

[3] Nguyen, Toan & Ho, Van & Do, Phuc. (2024). Optimizing Deep Learning for Skin Disease Classification: Leveraging Bayesian Hyperparameter Tuning and Top-K Accuracy Metrics. 10.1007/978-981-97-9613-7-8.

[4] Abed, Marwah Sameer Abed & Akbas, Ayhan. (2024). An Approach in Melanoma Skin Cancer Segmentation With Bat Optimization Algorithm. International Journal of Imaging Systems and Technology. 34. 10.1002/ima.23119.

[5] K., A.K., T.Y., S., Ahmed, S.T. et al. Trained neural networking framework based skin cancer diagnosis and categorization using grey wolf optimization. Sci Rep 14, 9388 (2024).

[6] Li Zhang, Sam Slade, Chee Peng Lim, Houshyar Asadi, Saeid Nahavandi, Haoqian Huang, Hang Ruan, Semantic segmentation using Firefly Algorithm-based evolving ensemble deep neural networks, Knowledge-Based Systems, Volume 277, 2023, 110828, ISSN 0950-7051.

[7] Hussein, A.A., Montaser, A.M., & Elsayed, H.A. (2025). Skin cancer image classification using hybrid quantum deep learning model with BiLSTM and MobileNetV2. Quantum Machine Intelligence, 7(1), 66.

[8] Kumar Lilhore, U., Simaiya, S., Sharma, Y.K., et al. (2024). A precise model for skin cancer diagnosis using hybrid U-Net and improved MobileNet-V3 with hyperparameters optimization. Scientific Reports, 14, 4299.

[9] Abohashish, S., Amin, H., & Elsedimy, E. (2025). Enhanced melanoma and non-melanoma skin cancer classification using a hybrid LSTM-CNN model. Scientific Reports, 15, Article 8954.

[10] Rao, A. J., Babu, M. R., DurgaRao, G., Kumar, G. P., & Lakshmanarao, A. (2024). Innovative Way of Identifying Skin Cancer Model Design with FCNN and LSTM. 2024 IEEE International Conference on Computing, Power and Communication Technologies (IC2PCT), Greater Noida, India, 287–291.

[11] Manivannan, G. S., Kaveri, K. B., Sinchana, A. R., Fathima, S., Sonika, T. M., & Priya, D. P. (2024). Performance Analysis of LSTM Classification Model from GLCM with Lion Optimization Algorithm Features for Melanoma Identification from Skin Cancer Images. 2024 International Conference on Computing and Intelligent Reality Technologies (ICCIRT), Coimbatore, India, 1–5.

[12] Mavaddati, S. (2025). Skin cancer classification based on a hybrid deep model and long short-term memory. Biomedical Signal Processing and Control, 100(Part A), 107109.

[13] Narendra, M., Harshini, T. S., & Anbarasi, L. J. (2024). Advancing skin disease diagnosis: A multimodal approach utilizing Telegram API token chatbot for text and image analysis in skin disease classification. IEEE Access, 12, 189009–189023.

[14] Padhy, S., Dash, S., Kumar, N., Singh, S. P., Kumar, G., & Moral, P. (2025). Temporal integration of ResNet features with LSTM for enhanced skin lesion classification. Results in Engineering, 25, 104201.

[15] Liu, H., Dou, Y., Wang, K., et al. (2025). A skin disease classification model based on multi scale combined efficient channel attention module. Scientific Reports, 15, 6116.

[16] Malik, S. G., Jamil, S. S., Aziz, A., Ullah, S., Ullah, I., & Abohashrh, M. (2024). High-Precision Skin Disease Diagnosis through Deep Learning on Dermoscopic Images. Bioengineering, 11(8), 867.

[17] A., J.C., A., U., V., R.M., et al. (2024). A novel CNN framework for skin disease classification using adaptive percentage filter for image binarization and fast-marching inpainting method. Multimedia Tools and Applications, 83, 63547–63570.

[18] Saha, D.K., Joy, A.M., & Majumder, A. (2024). YoTransViT: A transformer and CNN method for predicting and classifying skin diseases using segmentation techniques. Informatics in Medicine Unlocked, 47, 101495.

[19] Furqon, A., Malik, K., & Fajri, F. (2024). Detection of eight skin diseases using convolutional neural network with MobileNetV2 architecture for identification and treatment recommendation on Android application. Jurnal Ilmiah Teknik Elektro Komputer dan Informatika, 10(2), 373–384.

[20] Medhat, S., Abdel-Galil, H., Aboutabl, A.E. et al. Iterative magnitude pruning-based light-version of AlexNet for skin cancer classification. Neural Comput & Applic 36, 1413–1428 (2024).

[21] Djaroudib, K.; Lorenz, P.; Belkacem Bouzida, R.; Merzougui, H. Skin Cancer Diagnosis Using VGG16 and Transfer Learning: Analyzing the Effects of Data Quality over Quantity on Model Efficiency. Appl. Sci. 2024, 14, 7447.

[22] S. Ibrahim, K. M. Amin, R. I. Alkanhel, H. A. Abdallah, and M. Ibrahim, “Soft Attention Based EfficientNetV2B3 Model for Skin Cancer’s Disease Classification Using Dermoscopy Images,” IEEE Access, vol. 12, pp. 161283–161295, 2024.

[23] Alruwaili, M.; Mohamed, M. An Integrated Deep Learning Model with EfficientNet and ResNet for Accurate Multi-Class Skin Disease Classification. Diagnostics 2025, 15, 551.

[24] Noaman, A., Ahmad, R., Khan, M.F. et al. Beyond binary: multi-class skin lesion classification with AlexNet transfer learning-towards enhanced dermatological diagnosis. Discov Appl Sci 7, 35 (2025).

[25] S. RamaDevi, S. Sowjanya, Y. Hindu, C. S. Chakkavarapu and D. Rambabu, "DeepNet: Automated Skin Disease Classification using DenseNet for Accurate Dermatological Diagnosis," 2025 International Conference on Intelligent Computing and Control Systems (ICICCS), Erode, India, 2025, pp. 1365-1370.